

Deep Learning for Spatio-Temporal Modeling: Dynamic Traffic Flows and High Frequency Trading

Matthew F. Dixon
*Stuart School of Business
Illinois Institute of Technology**

Nicholas G. Polson
*Booth School of Business
University of Chicago*

Vadim O. Sokolov
*Systems Engineering and Operations Research
George Mason University*

First Draft: February 2017
This Draft: May 26th 2017

Abstract

Deep learning applies hierarchical layers of hidden variables to construct nonlinear high dimensional predictors. Our goal is to develop and train deep learning architectures for spatio-temporal modeling. Training a deep architecture is achieved by stochastic gradient descent (SGD) and drop-out (DO) for parameter regularization with a goal of minimizing out-of-sample predictive mean squared error. To illustrate our methodology, we predict the sharp discontinuities in traffic flow data, and secondly, we develop a classification rule to predict short-term futures market prices as a function of the order book depth. Finally, we conclude with directions for future research.

Keywords: Deep Learning, High Frequency Trading, Traffic Flow Prediction, Machine Learning, Bayes, Hyper-parameter tuning, Limit Order Book, Futures Markets.

*Matthew Dixon is an Assistant Professor in the Stuart Business School, Illinois Institute of Technology. E-mail: mdixon7@stuart.iit.edu. Nicholas Polson is Professor of Econometrics and Statistics at Chicago-Booth, University of Chicago. E-mail: ngp@chicagobooth.edu. Vadim Sokolov is an Assistant Professor in the Department of Systems Engineering and Operations Research, George Mason University. E-mail: vsokolov@gmu.edu

1 Introduction

Predicting spatio-temporal flows is a challenging problem as dynamic spatio-temporal data possess underlying complex interactions and nonlinearities. Deep learning applies layers of hierarchical hidden variables to capture these interactions and nonlinearities. The theoretical roots lie in the Kolmogorov-Arnold representation theorem (Arnold, 1957; Kolmogorov, 1957) of multivariate functions, which states that any continuous multivariate function can be expressed as a superposition of continuous univariate semi-affine functions. This remarkable result has direct consequences for statistical modeling as a non-parametric pattern matching algorithm. Deep learning relies on pattern matching via its layers of univariate semi-affine functions and can be applied to both regression and classification problems. Deep learners provide a nonlinear predictor in complex settings where the input space can be very high dimensional. The deep learning paradigm for data analysis is therefore algorithmic rather than probabilistic, see (Breiman, 2001).

Traditional statistical modeling approaches use a data generating process, generally motivated by physical laws or constraints. For example, spatio-temporal flow modeling uses physical models to describe the evolution of flows (Cressie & Wikle, 2015; Richardson, Kottas, & Sansó, 2017). The application of deep layers is central to our approach and builds on the previous work of (Higdon, 1998; Stroud, Müller, & Sansó, 2001; Wikle, Milliff, Nychka, & Berliner, 2001). The advantage of using deep layers with large amounts of training data is that nonlinearities and complex interactions can be discovered at different time scales.

To illustrate our methodology, we provide two applications (i) predicting the sharp discontinuities in short-term traffic flows that arise from the regime shift in free flow to congestion and (ii) classifying short-term price movements from a limit order book of financial futures market data. Both applications exhibit sharp regime changes which are hard to capture with traditional modeling techniques.

Training a deep learning architecture can be performed with stochastic gradient descent (SGD) which learns the weights and offsets in an architecture between the layers. Drop-out (DO) performs variable selection (Srivastava, Hinton, Krizhevsky, Sutskever, & Salakhutdinov, 2014). Deep learning (DL) relies on having a large amount of training data together with a flexible architecture to 'match' in and out of sample performance as measured by mean error, area under the curve (AUC) or the F1 score, which is the harmonic mean of precision and recall.

The rest of our paper is outlined as follows. Section 2 provides a statistical perspective on deep learning and outlines the training, validating and testing process required to construct a deep learner. Section 3 describes dynamic spatio-temporal modeling with deep learning. Section 4 describes the deep learning model of (Polson & Sokolov, 2016) for predicting short-term traffic flows. We provide a description of the spatio-temporal formulation of the deep learning model of (Dixon, Klabjan, & Bang, 2016; Sirignano, 2016). We quantify the empirical gains using a deep learner, to capture discontinuities and nonlinearities in the price movements, versus the elastic net method are quantified. Finally, Section 5 concludes with directions for future research.

2 Deep Learning

Deep learning is a form of machine learning that addresses a fundamental prediction problem: Construct a nonlinear predictor, $\hat{Y}(X)$, of an output, Y , given a high dimensional input matrix $X = (X_1, \dots, X_p)$. Machine learning can be simply viewed as the study and construction of an input-output map of the form

$$Y = F(X) \text{ where } X = (X_1, \dots, X_p).$$

The output variable, Y , can be continuous, discrete or mixed. For example, in a classification problem, $F : X \rightarrow Y$ where $Y \in \{1, \dots, K\}$ and K is the number of categories.

A deep predictor is a particular class of multivariate functions $F(X)$ that are generated by the superposition of univariate semi-affine functions. A semi-affine function, denoted by f_{W^l, b^l}^l , is defined as

$$f_{W^l, b^l}^l(X) := f^l(W^l X + b^l)$$

where f^l is univariate and continuous. A non-linear predictor is constructed using a sequence of layers L via a composite map

$$\hat{Y}(X) := F_{W,b}(X) = \left(f_{W^L, b^L}^L \dots \circ f_{W^1, b^1}^1 \right) (X).$$

Here $W = (W^1, \dots, W^L)$ and $b = (b^1, \dots, b^L)$ are weight matrices and offsets respectively. Deep learners form a universal basis due to the Kolmogorov-Arnold representation theorem (Kolmogorov, 1957; Arnold, 1957).

Let Z^l denote the l -th layer with $Z^0 = X$. The structure of a deep prediction rule can then be written as a hierarchy of $L - 1$ unobserved layers, Z^l , given by

$$\begin{aligned} \hat{Y}(X) &= f^L(Z^{L-1}), \\ Z^1 &= f^1(W^1 Z^0 + b^1), \\ Z^2 &= f^2(W^2 Z^1 + b^2), \\ &\dots \\ Z^{L-1} &= f^{L-1}(W^{L-1} Z^{L-2} + b^{L-1}). \end{aligned}$$

When Y is numeric, the output function $f^L(X)$ is given by the semi-affine function $f^L(X) := f_{W^L, b^L}^L(X)$. When Y is categorical, $f^L(X)$ is a softmax function. The activation (or link) functions, f^l , $1 \leq l < L$, are pre-specified where as the weight matrices $W^l \in \mathbf{R}^{N_l \times N_{l-1}}$ and offset vectors $b^l \in \mathbf{R}^{N_l}$ have to be learned from a training dataset $(Y^i, X^i)_{i=1}^T$. Common choices of f^l are hinge or rectified linear units, $\max(x, 0)$, and sigmoidal ($\cosh(x)$, $\tanh(x)$) activation functions. We will later discuss stochastic gradient descent (SGD) and the proximal Newton method described in Section 2.2.

The first stage in our architecture performs variable selection is to reduce the dimensionality of the problem. We first use a vector-autoregressive model or an elastic-net

model (Zou & Hastie, 2005) to perform a regularized fit to find the low dimensional parameter space. For our traffic flows data, we pre-processed with lasso and for our high frequency data with an elastic net. Multi-layer deep learning network is then used to model the nonlinear spatio-temporal patterns.

There are a number of issues in any architecture design. How many layers? How many neurons N_i in each hidden layer? How to perform 'variable selection'? Many of these problems can be solved by a stochastic search technique, called dropout (Srivastava et al., 2014), which we discuss in Section 2.3. Figure 1 shows a number of commonly used structures; for example, feed-forward architectures, neural Turing machines. Once you have learned the dimensionality of the weight matrices which are non-zero, there's an implied network structure.

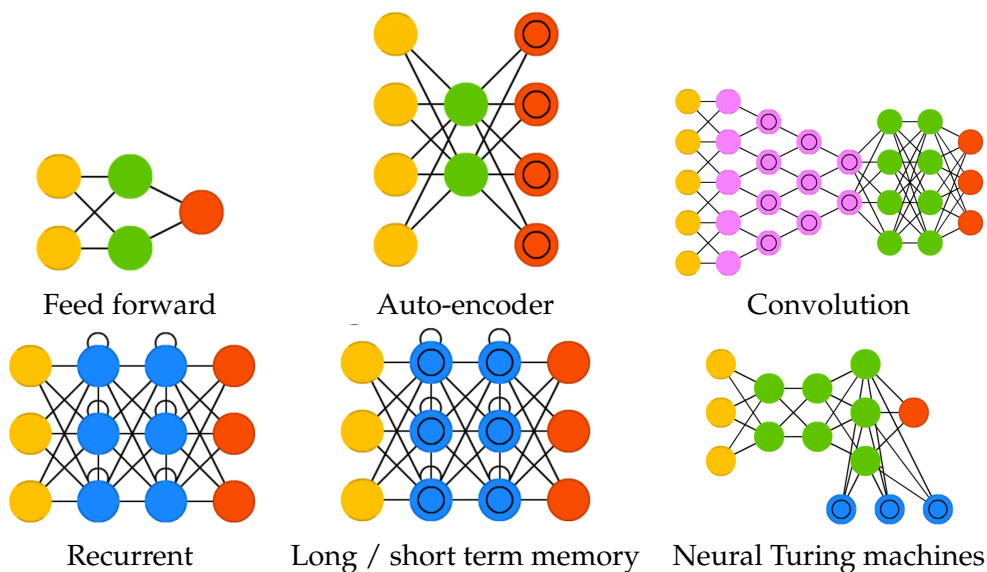


Figure 1: *Most commonly used deep learning architectures for modeling.* Source: <http://www.asimovinstitute.org/neural-network-zoo>.

2.1 Training, Validation and Testing

Deep learning is a data-driven approach which focuses on finding structure in large data sets. The main tools for variable or predictor selection are regularization and dropout. Out-of-sample predictive performance helps assess the optimal amount of regularization, the problem of finding the optimal hyper-parameter selection. There is still a very Bayesian flavor to the modeling procedure and the researcher follows two key steps:

1. Training phase: pair the input with expected output, until a sufficiently close match has been found. Gauss' original least squares procedure is a common example.
2. Validation and test phase: assess how well the deep learner has been trained for out-of-sample prediction. This depends on the size of your data, the value you

would like to predict, the input, etc., and various model properties including the mean-error for numeric predictors and classification-errors for classifiers.

Often, the validation phase is split into two parts.

- 2.a First, estimate the out-of-sample accuracy of all approaches (a.k.a. validation).
- 2.b Second, compare the models and select the best performing approach based on the validation data (a.k.a. verification).

Step 2.b. can be skipped if there is no need to select an appropriate model from several rivaling approaches. In this case, the researcher need only partition the data set into a training and test set.

To construct and evaluate a learning machine, we start with training data of input-output pairs $D = \{Y^{(i)}, X^{(i)}\}_{i=1}^T$. The goal is to find the machine learner $Y = F(X)$, where we have a loss function $\mathcal{L}(Y, \hat{Y})$ for a predictor, \hat{Y} , of the output signal, Y . In many cases, there's an underlying probability model, $p(Y | \hat{Y})$, then the loss function is the negative log probability $\mathcal{L}(Y, \hat{Y}) = -\log p(Y | \hat{Y})$. For example, under a Gaussian model $\mathcal{L}(Y, \hat{Y}) = \|Y - \hat{Y}\|^2$ is a L^2 norm, for binary classification, $\mathcal{L}(Y, \hat{Y}) = -Y \log \hat{Y}$ is the negative cross-entropy. In its simplest form, we then solve an optimization problem

$$\begin{aligned} & \underset{W, b}{\text{minimize}} f(W, b) + \lambda \phi(W, b) \\ f(W, b) &= \frac{1}{T} \sum_{i=1}^T \mathcal{L}(Y_i, \hat{Y}(X_i)) \end{aligned}$$

with a regularization penalty, $\phi(W, b)$. Here λ is a global regularization parameter which we tune using the out-of-sample predictive mean-squared error (MSE) of the model. The regularization penalty, $\phi(W, b)$, introduces a bias-variance tradeoff. $\nabla \mathcal{L}$ is given in closed form by a chain rule and, through back-propagation, each layer's weights \hat{W}^l are fitted with stochastic gradient descent.

2.2 Stochastic gradient descent (SGD)

Stochastic gradient descent (SGD) method or its variation is typically used to find the deep learning model weights by minimizing the penalized loss function, $f(W, b)$. The method minimizes the function by taking a negative step along an estimate g^k of the gradient $\nabla f(W^k, b^k)$ at iteration k .

The approximate gradient is estimated by calculating

$$g^k = \frac{1}{b_k} \sum_{i \in E_k} \nabla \mathcal{L}_{W, b}(Y_i, \hat{Y}^k(X_i)),$$

where $E_k \subset \{1, \dots, T\}$ and $b_k = |E_k|$ is the number of elements in E_k (a.k.a. batch size). When $b_k > 1$ the algorithm is called batch SGD and simply SGD otherwise. A usual strategy to choose subset E is to go cyclically and pick consecutive elements of

$\{1, \dots, T\}$ and $E_{k+1} = [E_k \bmod T] + 1$. The approximated direction g^k is calculated using a chain rule (a.k.a. back-propagation) for deep learning. It is an unbiased estimator of $\nabla f(W^k, b^k)$, and we have

$$E(g^k) = \frac{1}{T} \sum_{i=1}^T \nabla \mathcal{L}_{W,b}(Y_i, \hat{Y}^k(X_i)) = \nabla f(W^k, b^k).$$

At each iteration, the SGD updates the solution

$$(W, b)^{k+1} = (W, b)^k - t_k g^k.$$

In deep learning applications the step size t_k (a.k.a. learning rate) is typically kept constant or a step size reduction strategy is used, $t_k = a \exp(-kt)$. Appropriate learning rates or the hyper-parameters of reduction schedule are usually found empirically from numerical experiments and observations of the loss function progression.

One disadvantage of SGD is that the descent in f is not guaranteed or can be very slow at every iteration. Further, the variance of the gradient estimate g^k is near zero as the iterates converge to a solution. To tackle those problems a coordinate descent (CD) and momentum-based modifications of SGD are used.

Each CD step evaluates a single component E_k of the gradient ∇f at the current point and then updates the E_k th component of the variable vector in the negative gradient direction. The momentum-based versions of SGD or so-called accelerated algorithms were originally proposed by (Nesterov, 2013). The use of momentum in the choice of step in the search direction combines new gradient information with the previous search direction. These methods are also related to other classical techniques such as the heavy-ball method and conjugate gradient methods. Empirically momentum-based methods show a far better convergence for deep learning networks. The key idea is that the gradient only influences changes in the "velocity" of the update

$$\begin{aligned} v^{k+1} &= \mu v^k - t_k g^k, \\ (W, b)^{k+1} &= (W, b)^k + v^k. \end{aligned}$$

The parameter μ controls the dumping effect on the rate of update of the variables. The physical analogy is the reduction in kinetic energy that allows "slow down" the movements at the minima. This parameter is also chosen empirically using cross-validation.

Nesterov's momentum method (a.k.a. Nesterov acceleration) instead calculate gradient at the point predicted by the momentum. We can think of it as a look-ahead strategy. The resulting update equations are

$$\begin{aligned} v^{k+1} &= \mu v^k - t_k g((W, b)^k + v^k), \\ (W, b)^{k+1} &= (W, b)^k + v^k. \end{aligned}$$

Another popular modification to the SGD method is the AdaGrad method, which adap-

tively scales each of the learning parameters at each iteration

$$\begin{aligned} c^{k+1} &= c^k + g((W, b)^k)^2, \\ (W, b)^{k+1} &= (W, b)^k - t_k g(W, b)^k / (\sqrt{c^{k+1}} - a), \end{aligned}$$

where a is usually a small number, e.g. $a = 10^{-6}$ that prevents dividing by zero. PRM-Sprop takes the AdaGrad idea further and places more weight on recent values of the gradient squared to scale the update direction, i.e. we have

$$c^{k+1} = dc^k + (1 - d)g((W, b)^k)^2.$$

The Adam method combines both PRMSprop and momentum methods and leads to the following update equations

$$\begin{aligned} v^{k+1} &= \mu v^k - (1 - \mu)t_k g((W, b)^k + v^k), \\ c^{k+1} &= dc^k + (1 - d)g((W, b)^k)^2, \\ (W, b)^{k+1} &= (W, b)^k - t_k v^{k+1} / (\sqrt{c^{k+1}} - a). \end{aligned}$$

Second order methods solve the optimization problem by solving a system of nonlinear equations $\nabla f(W, b) = 0$ with the Newton's method

$$(W, b)^+ = (W, b) - \{\nabla^2 f(W, b)\}^{-1} \nabla f(W, b).$$

SGD simply approximates $\nabla^2 f(W, b)$ by $1/t$. The advantages of a second order method include much faster convergence rates and insensitivity to the conditioning of the problem. In practice, second order methods are rarely used for deep learning applications (Dean et al., 2012). The major disadvantage is the inability to train the model using batches of data as SGD does. Since typical deep learning models relies on large scale data sets, second order methods become memory and computationally prohibitive at even modest-sized training data sets.

However batching alone is not sufficient to scale SGD methods to large-scale problems on modern high performance computers. Back-propagation through a chain-rule creates an inherit sequential dependency in the weight updates which limits the dataset dimensions for the deep learner. (Polson, Willard, & Heidari, 2015) consider a proximal Newton method, a Bayesian optimization technique which provides an efficient solution for estimation and optimization of such models and for calculating a regularization path. The authors present a splitting approach, alternating direction method of multipliers (ADMM), which overcomes the inherent bottle-necks in back-propagation by providing a simultaneous block update of parameters at all layers. ADMM facilitates the use of large-scale computing.

A significant factor in the widespread adoption of deep learning has been the creation of `TensorFlow` (Abadi et al., 2016), an interface for easily expressing machine learning algorithms and mapping compute intensive operations onto a wide variety of different hardware platforms and in particular GPU cards. Recently, `TensorFlow` has

been augmented by Edward (Tran et al., 2017) to combine concepts in Bayesian statistics and probabilistic programming with deep learning.

2.3 Predictor Selection and Dropout

Dropout is a model or variable selection technique. The input space $X = (X_1, \dots, X_p)$, where p is large, needs dimension reduction techniques which are designed to avoid over-fitting in the training process. Dropout works by removing input dimensions in X randomly with a given probability θ . The probability, θ , can be viewed as a further hyper-parameter (like λ) which can be tuned via cross-validation. Heuristically, if there are 1000 variables, then a choice of $\theta = 0.1$ will result in a search for models with 100 variables. The dropout architecture with stochastic search for the predictors can be used

$$\begin{aligned} D_i^l &\sim \text{Ber}(\theta), \\ \tilde{Z}^l &= D^l \star Z^l, \quad 1 \leq l < L, \\ Z^l &= f^l(W^l \tilde{Z}^{l-1} + b^l). \end{aligned}$$

Effectively, this replaces the input X by $D \star X$, where \star denotes the element-wise product and D is a vector of independent Bernoulli $\text{Ber}(\theta)$ distributed random variables. The overall objective function is closely related to ridge regression with a g-prior (Heaton, Polson, & Witte, 2017).

3 Dynamic Spatio-Temporal Modeling (DSTM)

Suppose that we have data at spatial locations $s_i, i = 1, \dots, n$ and time t . Denote this by the process $Y_t = \{Y(s_i, t)\}_{i=1}^n$. The goal is to predict at a particular location, and forecast at a new time point given training data. Denote this quantity by $Y(s^*, t^*)$. A simple linear predictor would take the form as a 'local' average of 'near-by' points denoted by

$$\hat{Y}(s^*, t^*) = \sum_{i=1}^n \sum_{j=1}^T w_{ij}^* Y(s_i, t_j). \quad (1)$$

Deep learning simply uses a hierarchical layered predictor with univariate activation functions and weight matrices of different dimensions to capture the complex interactions that exist in the evolution of the process in space and time. Typical architectures (connecting non-zero weights) include traditional recurrent neural networks (RNNs), convolutional neural networks and, more recently, long short term memory (LSTM) models.

Rather than directly imposing a covariance structure (e.g. Gaussian process with $O(n^3)$ parameters (Gramacy & Polson, 2011)), a deep learner provides a flexible functional form to directly model the predictor, \hat{Y} . Parameter search is then achieved by regularizing a measure of fit and the optimal amount of regularization is achieved by measuring the out-of-sample bias-variance trade-off in a hold-out sample. Underlying

this approach is the assumption that we have sufficient data to ‘train’ a predictor that captures the hidden complex interactions. For example, a ‘vanilla’ RNN might look something like

$$\begin{aligned} \text{response:} & \quad \hat{Y}_t = \text{softmax}(Z_t^2), \\ \text{activation output:} & \quad Z_t^2 = f(W_z^2 Z_t^1 + b^2), \\ \text{hidden states:} & \quad Z_t^1 = \max(W_z^1 Z_{t-1}^1 + W_x^1 X_t + b^1, 0), \end{aligned}$$

where f is an activation function such as $\tanh(x)$ and the time invariant weight matrices are W_z^1 , W_z^2 and W_x^1 . X_t are extremal inputs and Z_{t-1}^1 is a matrix of past process states $Y_{t-1, \dots, t-k}$ and k is the degree of memory in our model. The size of Z_{t-1}^1 in our applications is generally from a few hundred rows to a few thousand.

The power of deep learners is that we can use the multiple hidden layers. Think of each layer as a local filter that captures a complex interaction on some space, time scale.

4 Applications

4.1 Predicting Traffic Flow Data

To illustrate our methodology, we use data from twenty-one loop-detectors installed on a northbound section of Interstate I-55 which span 13 miles of the highway¹. The data is measured by loop-detector sensors installed on interstate highways. A loop-detector is a presence sensor that measures when a vehicle is present and generates an on/off signal. Since 2008, Argonne National Laboratory has been archiving traffic flow data every five minutes from the grid of sensors recording averaged *speed*, *flow*, and *occupancy*. Occupancy is defined as the percentage of time a point on the road is occupied by a vehicle, and flow is the number of on-off switches. Illinois uses a single loop detector setting, and speed is estimated based on the assumption of an average vehicle length.

Finding the spatio-temporal relations in the data is the predictor selection problem. Figure 2 illustrates a space-time diagram of traffic flows on a 13-mile stretch of highway I-55 in Chicago. You can see a clear spatio-temporal pattern in traffic congestion propagation in both downstream and upstream directions. The spatio-temporal data can be represented as

$$Y = x_{t+40}^t = \begin{pmatrix} x_{1,t+40} \\ \vdots \\ x_{n,t+40} \end{pmatrix},$$

x_{t+h}^t is the forecast of traffic flow speeds at time $t+h$, given measurements up to time t .

¹Traffic flow data is available from the Illinois Department of Transportation, (see Lake Michigan Interstate Gateway Alliance <http://www.travelmidwest.com/>, formally the Gary-Chicago-Milwaukee Corridor, or GCM).

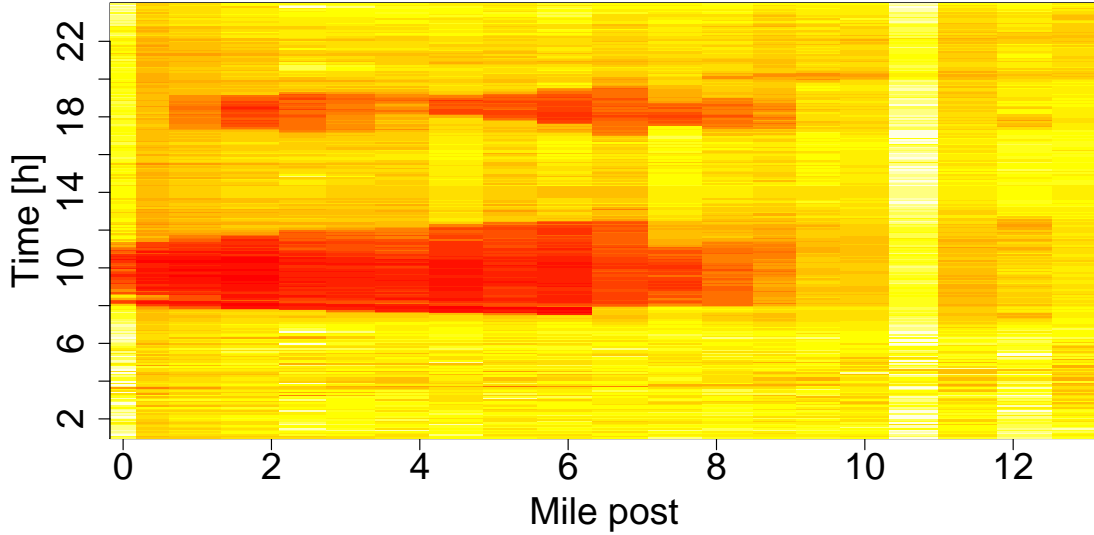


Figure 2: A space-time diagram that shows traffic flow speed over a 13-mile stretch of I-55 on 18 February 2009 (Wednesday). Red represents slow speed and light yellow corresponds to free flow speed. The direction of the flow is from 0 to 13.

For the traffic flow model previously measured and possibly filtered traffic flow data given by $x^t = (x_{t-k}, \dots, x_t)$ used as predictors

$$x = x^t = \text{vec} \begin{pmatrix} x_{1,t-40} & \dots & x_{1,t} \\ \vdots & \vdots & \vdots \\ x_{n,t-40} & \dots & x_{n,t} \end{pmatrix}.$$

Here n is the number of locations on the network (loop detectors) and $x_{i,t}$ is the cross-sectional traffic flow speed at location i at time t . vec is the vectorization transformation which converts the matrix into a column vector. In our application examined later in Section 4.2, we have twenty-one road segments (i.e., $n = 21$) that span thirteen miles of a major corridor connecting Chicago's southwest suburbs to the central business district. The chosen length is consistent with several current transportation corridor management deployments (TransNet, 2016).

Our layers are constructed as follows, $z^0 = x$, then $z^l, l = 1, \dots, L$ is a time series "filter" given by

$$z^l = f(W^l z^{l-1} + b^l).$$

Here $z^{l-1} \in \mathbb{R}^{N_{l-1}}$ denotes a vector of inputs into a layer l and N_l is the number of activation units (neurons) in layer l and function f is called an activation function.

A predictor selection problem requires estimation algorithms for finding sparse models. Those rely on adding a penalty term to a loss function. A recent review by (Nicholson,

Matteson, & Bien, 2017) considers several prominent scalar regularization terms to identify sparse vector auto-regressive models.

First we construct a hierarchical linear vector autoregressive model to identify the spatio-temporal relations in the data. We consider the problem of finding sparse matrix, W^0 , in the following model

$$x_{t+40}^t = W^0 x^t + \epsilon_t, \quad \epsilon_t \sim N(0, V);$$

where W^0 is a matrix of size $n \times nk$, and k is the number of previous measurements used to develop a forecast. In our example in Section 4.2, we have $n = 21$; however, in large scale networks, there are tens of thousands locations with measurements available.

The predictors selected as a result of finding the linear model are then used to build a deep learning model. To find an optimal network (structure and weights) we used the SGD method implemented in the package `H2O`. Similar methods are available in Python’s `Theano` (Bastien et al., 2012) or `TensorFlow` (Abadi et al., 2016) framework. We use random search to find meta parameters of the deep learning model. To illustrate our methodology, we generated $N = 10^5$ Monte Carlo samples from the following space:

$$\begin{aligned} \text{response:} & \quad \hat{Y}_t = W^L Z^{L-1} + b^L, \\ \text{hidden states:} & \quad Z^l = \tanh(W^l Z^{l-1} + b^l), \quad 1 \leq l < L, \end{aligned}$$

where $L = 4$.

To find the optimal structure of the neural network (number of hidden layers L , number of activation units in each layer N_l and activation functions f) as well as hyper-parameters, such as ℓ_1 regularization weight, we used a random search. Though this technique can be inefficient for large scale problems, for the sake of exploring potential structures of the networks that deliver good results and can be scaled, this is an appropriate technique for small dimensions. Stochastic gradient descent used for training a deep learning model scales linearly with the data size. Thus the hyper-parameter search time is linear with respect to model size and data size. On a modern processor it takes about two minutes to train a deep learning network on 25,000 observations of 120 variables. Hyper-parameter tuning and model structure search requires the model to be fit 10^5 times. Thus the total wall-time (time that elapses from start to end) was 138 days. An alternative to random search for learning the network structure for traffic forecasts was proposed in (Vlahogianni, Karlaftis, & Golias, 2005) and relies on the genetic optimization algorithm.

4.2 Traffic Flow on Chicago’s Interstate I-55

One of the key attributes of congestion propagation on a traffic network is the spatial and temporal dependency between bottlenecks. For example, if we consider a stretch of highway and assume a bottleneck, than it is expected that the end of the queue will

move from the bottleneck downstream. Sometimes, both the head and tail of the bottleneck move downstream together. Such discontinuities in traffic flow, called shock waves are well studied and can be modeled using a simple flow conservation principles. However, a similar phenomena can be observed not only between downstream and upstream locations on a highway. A similar relationship can be established between locations on city streets and highways (Horvitz, Apacible, Sarin, & Liao, 2012).

An important aspect of traffic congestion is that it can be 'decomposed' into recurrent and non-recurrent factors. For example, a typical commute time from a western suburb to Chicago's city center on Mondays is 45 minutes. However, occasionally the travel time is 10 minutes shorter or longer. Figure 3(a) shows measurements from all non-holiday Wednesdays in 2009. The solid line and band, represent the average speed and 60% confidence interval correspondingly. Each dot is an individual speed measurement that lies outside of 98% confidence interval. Measurements are taken every five minutes, on every Wednesday of 2009; thus, we have roughly 52 measurements for each of the five-minute intervals.

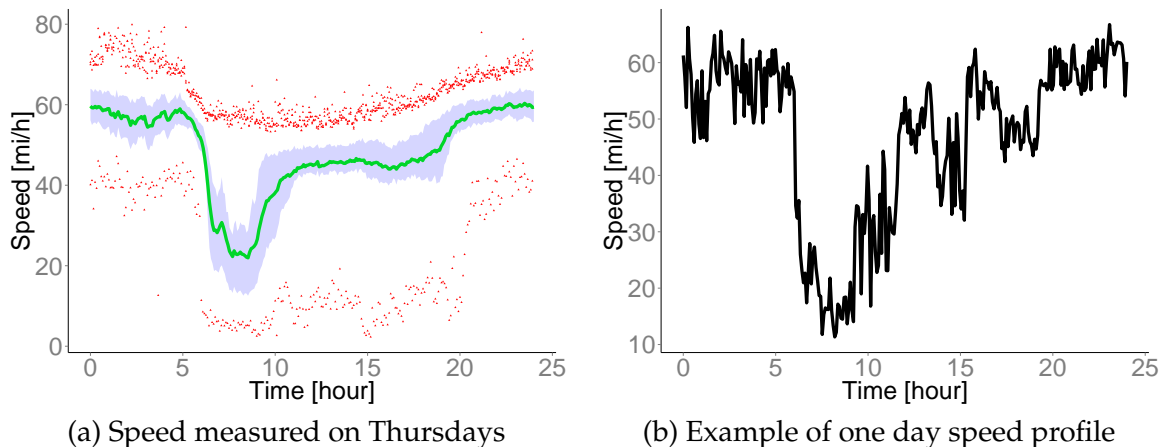


Figure 3: Recurrent speed profile. Both plots show the speed profile for a segment of interstate highway I-55. Left panel (a) shows the green line, which is the average cross-section speed for each of five minute intervals with 60% confidence interval. The red points are measurements that lie outside of 98% confidence interval. Right panel (b) shows an example of one day speed profile from May 14, 2009 (Thursday).

We see that in many cases traffic patterns are very similar from one day to another. However, there are many days when we see surprises, both good and bad. A good surprise might happen, e.g., when schools are closed due to extremely cold weather. A bad surprise might happen due to non-recurrent traffic conditions, such as an accident or inclement weather.

Figure 4 shows the impact of non-recurrent events. In this case, the traffic speed can significantly deviate from historical averages due to the increased number of vehicles on the road or due to poor road surface conditions.

Our goal is to build a statistical model to capture the sudden regime changes from

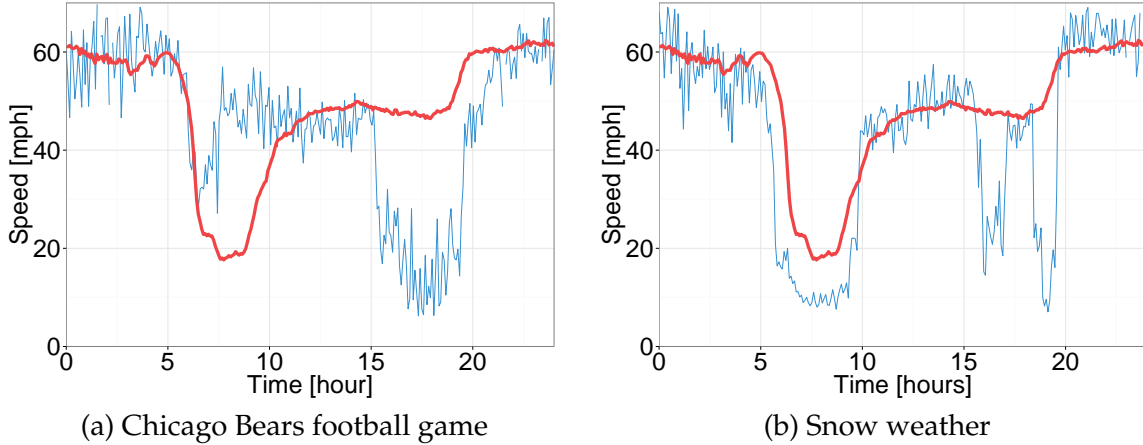


Figure 4: *Impact of non-recurrent events on traffic flows. Left panel (a) shows traffic flow on a day when New York Giants played at Chicago Bears on Thursday October 10, 2013. Right panel (b) shoes impact of light snow on traffic flow on I-55 near Chicago on December 11, 2013. On both panels average traffic speed is red line and speed on event day is blue line.*

free flow to congestion and then the decline in speed to the recovery regime for both recurrent traffic conditions and non-recurrent ones.

Both deep learning (DL) and vector auto-regressive (VAR) models accurately predict the morning rush hour congestion on a normal day. However, the vector auto-regressive model mis-predicts congestion during evening rush hour. At the same time, the deep learning model does predict breakdown accurately but miss-estimates the time of recovery. Both deep learning and linear model outperform naive forecasting when combined with data pre-processing. However, when unfiltered data is used to fit deep learning combined with a sparse linear estimator (DLL) model, their predictive power degrades and were out-performed by a naive forecast. Thus, showing the importance of using filtered data to develop forecasts.

4.3 Predicting Short-term Futures Prices from High Frequency Data

Modern financial markets facilitate the electronic trading of financial instruments through an instantaneous double auction. At each point in time, the market demand and the supply can be represented by an electronic limit order book, a cross section of orders to execute at various price levels away from the market price.

The market price is closely linked to its liquidity - that is the immediacy in which the instrument can be converted into cash. The liquidity of markets are characterized by their depth, the total quantity of quoted buy and sell orders about the market price. Liquid markets are attractive to market participants as they permit the near instantaneous execution of large volume trades at the best available price, with marginal price impact. A participant enters into a trade by submitting an order to a queue and either waits up to a few milliseconds for the order to be filled or cancels the order. This type of trading adds liquidity and is said to be 'making a market', a primary function of high frequency

trading firms. A participant willing to pay a premium to trade at the best price can by pass the queue and is said to be ‘market taking’. The liquidity of the market evolves in response to trading activity (Bloomfield, O’Hara, & Saar, 2005); At any point in time, the amount of liquidity in the market can be characterized by the cross-section of book depths. The price levels closest to the market price define the ‘inside market’ and is the most actively traded.

The field of microstructure research (Parlour, 1998; Cao, Hansch, & Wang, 2009; Cont, Kukanov, & Stoikov, 2014) has established a causal relationship between the depth of the inside market and the market price through temporal models of order flow imbalance. There is growing evidence that the study of microstructure is critical to studying longer term relations and even cross-market effects (Dobrislav & Schaumburg, 2016).

Recently microstructure researchers have looked beyond the inside market to predict the price movement. Most notably, (Kozhan & Salmon, 2012), use a series of independent regressions to forecast each price level. The link between dynamic spatio-temporal models is demonstrated here. We build on previous machine learning algorithms for futures price predictions with high frequency data (Dixon et al., 2016; Sirignano, 2016).

4.4 High Frequency Futures Data

Our dataset is an archived Chicago Mercantile Exchange (CME) FIX format message feed captured from August 1, 2016 to August 31, 2016. This message feed records all transactions in the E-mini S&P 500 (ES) between the times of 12:00pm and 22:00 UTC. We extract details of each limit order book update, including the nano-second resolution time-stamp, the quoted price and depth for each limit order book level.

Figure 5 illustrates the intuition behind a typical mechanism resulting in mid-price movement. We restrict consideration to the top five levels of the ES futures limit order book, even though there are updates provided for ten levels. The chart on the left represents the state of the limit order book prior to the arrival of a sell aggressor. The x-axis represents the price levels and the y-axis represents the depth of book at each price level. Red denotes bid orders and blue denotes ask orders. The highest bid price (‘best bid’) is quoted at \$2175.75 with a depth of 103 contracts. The second highest bid is quoted at \$2175.5 with a depth of 177 contracts. The lowest ask (‘best ask’ or ‘best offer’) is quoted at \$2176 with 82 contracts and the second lowest ask is quoted at \$2176.25 with 162 contracts.

The chart on the right shows the book update after a market crossing limit order (‘aggressor’) to sell 103 contracts at \$2175.75. The aggressor is sufficiently large to match all of the best bids. Once matched, the limit order is updated with a lower best bid of \$2175.5. The gap between the best ask and best bid would widen if it weren’t for the arrival of 23 new contracts offered at a lower ask price of \$2175.75. The net effect is a full down-tick of the mid-price.

Table 1 shows the corresponding spatio-temporal representation of the limit order book before and after the arrival of the sell aggressor. The response is mid-price movement, in units of ticks, over the subsequent interval. $p_{i,t}^b$ and $d_{i,t}^b$ denote the level i quoted

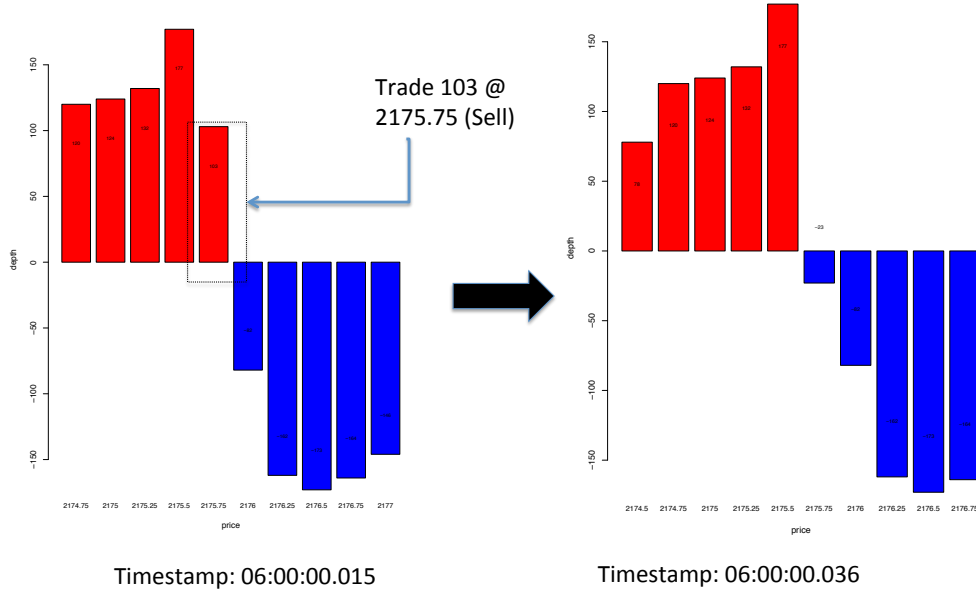


Figure 5: This figure illustrates a typical mechanism resulting in mid-price movement. The charts on the left and right respectively show the limit order book before and after the arrival of a large sell aggressor. The aggressor is sufficiently large to match all of the best bids. Once matched, the limit order is updated with a lower best bid of \$2175.5. The gap between the best ask and best bid would widen if it weren't for the arrival of 23 new contracts offered at a lower ask price of \$2175.75. The net effect is a full down-tick of the mid-price.

bid price and depth of the limit order book at time t . $p_{i,t}^a$ and $d_{i,t}^a$ denote the corresponding level i quoted ask price and depth. Level $i = 1$ corresponds to the best ask and bid prices. The mid-price at time t is denoted by

$$p_t = \frac{p_{1,t}^a + p_{1,t}^b}{2}. \quad (2)$$

This mid-price can evolve in minimum increments of half a tick but almost always is observed to move at increments of a tick over time intervals of a milli-second or less.

The result of categorizing (a.k.a. labeling) the data leads to a class imbalance problem as approximately 99.9% of the observations have a zero response. This imbalance can be partially resolved by under-sampling the data at regular intervals, an approach referred to as 'clocking'. However, the imbalance is still too severe for robust classification and clocking the data set reduces the predictive power of the models. To construct a 'balanced' training set, the minority classes are oversampled with replacement and the

Timestamp	$p_{1,t}^b$	$p_{2,t}^b$...	$d_{1,t}^b$	$d_{2,t}^b$...	$p_{1,t}^a$	$p_{2,t}^a$...	$d_{1,t}^a$	$d_{2,t}^a$...	Response
06:00:00.015	2175.75	2175.5	...	103	177	...	2176	2176.25	...	82	162	...	-1
06:00:00.036	2175.5	2175.25	...	177	132	...	2175.75	2176	...	23	82	...	0

Table 1: This table shows the corresponding spatio-temporal representation of the limit order book before and after the arrival of the sell aggressor listed in Figure 5. The response is the mid-price movement over the subsequent interval, in units of ticks. $p_{i,t}^b$ and $d_{i,t}^b$ denote the level i quoted bid price and depth of the limit order book at time t . $p_{i,t}^a$ and $d_{i,t}^a$ denote the corresponding level i quoted ask price and depth.

majority class is undersampled without replacement. The resulting balanced training set has 298062 observations for ESU6.

Our model of mid-price impact is described as follows. The response is

$$Y = \Delta p_{t+h}^t, \quad (3)$$

where Δp_{t+h}^t is the forecast of discrete mid-price changes from time t to $t + h$, given measurement of the predictors up to time t . When the historical data is clocked, h corresponds to the undersampling frequency. When the unclocked data is used, h denotes the inter-event arrival time and will vary with trading activity. The price impact model $\hat{Y}(X)$ uses relative market depth as the predictors

$$x = x^t = \text{vec} \begin{pmatrix} x_{1,t-k} & \dots & x_{1,t} \\ \vdots & & \vdots \\ x_{n,t-k} & \dots & x_{n,t} \end{pmatrix} \quad (4)$$

where n is the number of quoted price levels, k is the number of lagged observations, and $x_{i,t} \in [0, 1]$ is the relative depth, representing liquidity imbalance, at quote level i

$$x_{i,t} = \frac{d_{i,t}^b}{d_{i,t}^a + d_{i,t}^b}. \quad (5)$$

This price impact model captures the spatio-temporal relationship between mid-price movement and the liquidity imbalance across all levels of the limit order book. The CME futures data gives $n = 10$ quote levels on either side of the market, although other exchanges such as the NYSE may release quotes for hundreds of price levels.

Figure 6 shows a time-space diagram of the limit order book. The contemporaneous depth imbalances at each price level in the limit order book polarize prior to each price movement. The x axis shows the prices of each book level and the y-axis shows the timestamp of the limit order book at 1 second snapshots over a fifteen minute period from bottom to top. In a liquid market these prices move in unison, separated by a small increment referred to as a 'tick'. However, in periods of less liquidity, temporary perturbations in the price increments near the market price may exist and the price levels temporarily fall out-of-lock step with each other.

The color scale represents the liquidity imbalance relative to each price level. Red

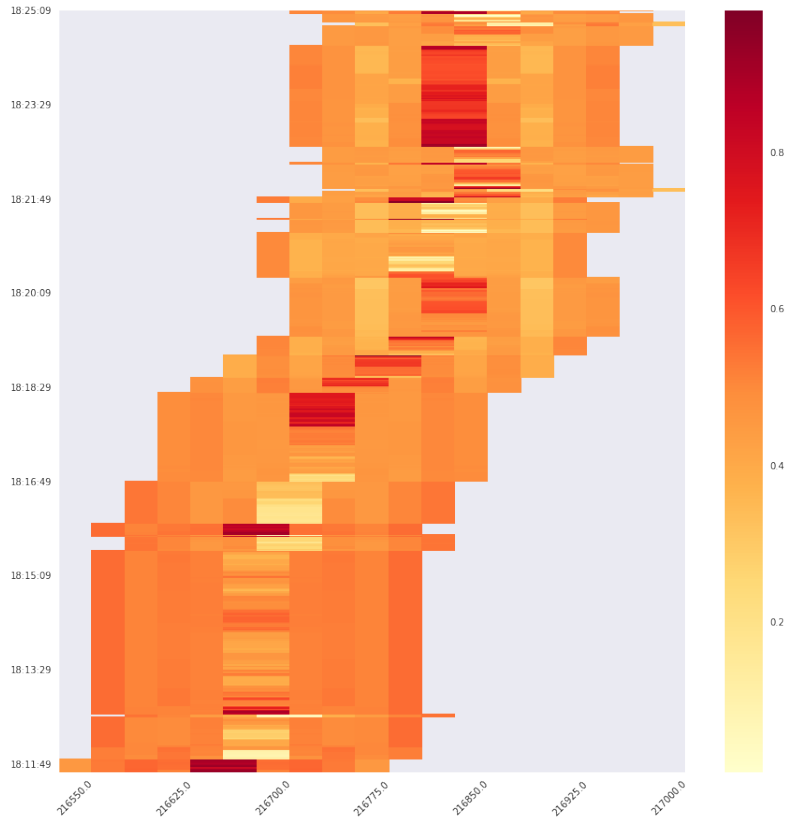


Figure 6: A space-time diagram showing the limit order book. The contemporaneous depths imbalances at each price level, $x_{i,t}$, are represented by the color scale: red denotes a high value of the depth imbalance and yellow the converse. The limit order book are observed to polarize prior to a price movement.

presents an excess of demand to supply and yellow the converse. With this spatio-temporal representation we may gain an appreciation as to why practitioners commonly refer to this imbalance as 'book pressure'. The book pressure at the inside market, 'the inside market pressure', is the strongest predictor of market price movement. More often than not, an upward price movement follows the cumulation of the inside market book pressure and, conversely, a downward price movement follows a depreciation of the inside market book pressure. Sometimes the full saturation or desaturation of the inside market pressure does not result in a price movement. This observation is consistent with various studies in different markets such as (Kozhan & Salmon, 2012). In using the cross-section of relative depths in the spatio-temporal model, rather than just the inside market, the deep learner is able to find relationships which lead to improved price impact forecasts, especially at the short time scales necessary for high frequency trading.

4.5 Deep Learner

Each categorical response Y_i is represented as a 1-of- K indicator vector, with all elements equal to zero except the element corresponding to the correct class k . For example, if $K = 3$ and the correct class is 1 then Y_i is represented as $[1, 0, 0]$.

The goal of our deep learner is to find the weights and bias terms which minimize the cross-entropy function

$$\hat{W}, \hat{b} = \underset{W, b}{\operatorname{argmin}} f(W, b) + \lambda \phi(W, b),$$

$$f(W, b) = \frac{1}{T} \sum_{i=1}^T \mathcal{L}(Y_i, \hat{Y}(X_i)),$$

with negative cross-entropy loss, corresponding to multi-class logistic regression,

$$\mathcal{L}(Y, \hat{Y}) = - \sum_{k=1}^K Y_k \log \hat{Y}_k. \quad (6)$$

The exact architecture and weight matrix sizes of our deep learner are given by

$$\text{response : } \hat{Y}_k = \operatorname{softmax}(Z^{(L-1)}) = \frac{\exp(Z_k^{(L-1)})}{\sum_{j=1}^K \exp(Z_j^{(L-1)})},$$

$$\text{hidden states : } Z^\ell = \max(W^\ell Z^{\ell-1} + b^\ell, 0), \quad 1 \leq \ell < L,$$

where $L = 5$ and the network is tapered so that $W^{(1)} \in \mathbb{R}^{300 \times 401}$, $W^{(2)} \in \mathbb{R}^{200 \times 300}$, $W^{(3)} \in \mathbb{R}^{100 \times 200}$, $W^{(4)} \in \mathbb{R}^{50 \times 100}$, $W^{(5)} \in \mathbb{R}^{3 \times 50}$.

We use the SGD method, implemented in Python's TensorFlow (Abadi et al., 2016) framework, to find the optimal network weights, bias terms and regularization parameters. We employ an exponentially decaying learning rate schedule with an initial value of 10^{-2} . The optimal ℓ_2 regularization is found, via a grid-search, to be $\lambda_2 = 0.01$. The Glorot and Bengio method is used to initialize the weights of the network (Glorot & Bengio, 2010).

Times series cross-validation is performed using an unbalanced validation and test set, each of size 2×10^5 observations. The out-of-sample model performance on the verification set is used as the criteria for selecting our final deep learning architecture. Each experiment is run for 2500 epochs with a mini-batch size of 32 drawn from the training set of 298,062 observations of 440 variables. These 440 variables are initially chosen from 10 liquidity imbalance ratios lagged up to 40 past observations and an additional lagged variable representing the relative size of the aggressors. Elastic-net ($\alpha = 0.5$), with a weight matrix $W_0 \in \mathbb{R}^{401 \times 440}$, is used for regularization and variable selection. The gridded search to find the optimal network architecture and regularization parameters takes several days on a graphics processing unit (GPU). The search yields several candidate architectures and parameter values.

Table 2 compares the performance of the deep learner with the elastic net method, implemented in the R package `glmnet` (Friedman, Hastie, & Tibshirani, 2010; Simon, Friedman, Hastie, & Tibshirani, 2011), for predicting the next price movement. The elastic-net method, with $\alpha = 0.5$, exhibits an out-of-sample classification accuracy of 49.6%. However, due to the imbalance of the data, we use the $F1$ score - the geometric mean of the precision and recall:

$$F1 = 2 \frac{\text{precision} \cdot \text{recall}}{\text{precision} + \text{recall}}.$$

The $F1$ score is designed for binary classification problems. When the data has more than two classes, the $F1$ score is provided for each class. The score is highest for the zero label corresponding to a prediction of a stationary mid-price over the next interval. The $F1$ scores for a predicted up-tick $F1(1)$ and down-tick $F1(-1)$ are also shown. The deep learners exhibit a higher accuracy of 81.7% and higher $F1$ scores for each class.

Model	F1 (-1)	F1(0)	F1 (1)	Accuracy
Elastic-Net	0.116	0.649	0.108	0.496
DL with Elastic-Net	0.201	0.897	0.186	0.817

Table 2: The $F1$ scores and classification accuracy are compared between the elastic net model and the combined deep learner and elastic net model. The deep learners exhibit a higher accuracy and higher $F1$ scores for each class.

Table 3 compares the Receiver Operator Characteristic (ROC) curves for the deep learner and the elastic net method for (left) downward, (middle) neutral, or (right) upward price prediction. The plot is constructed by varying the probability threshold (a.k.a. cut-points) for positive classification over the interval $[0.5, 1)$ and estimating the true positive and true negative rate of each model. In each case, the deep learner is observed to out-perform the elastic net method. The dashed line shows the performance of a white-noise classifier.

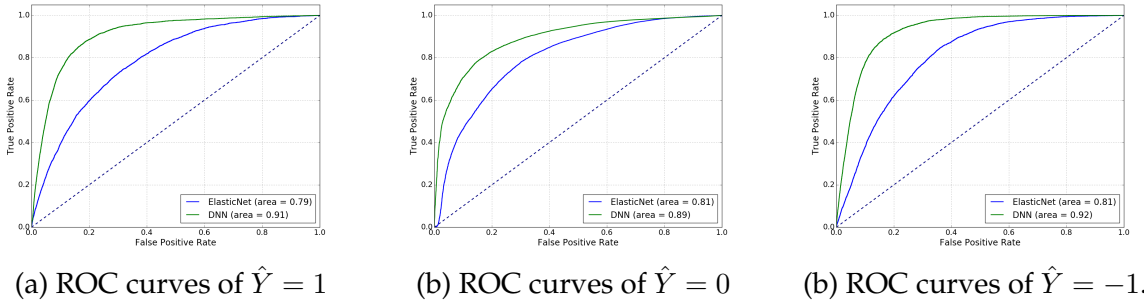
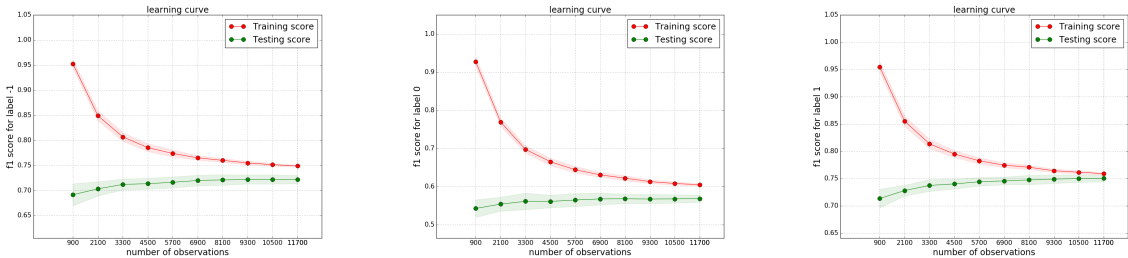


Table 3: The Receiver Operator Characteristic (ROC) curves of the deep learner and the elastic net method are shown for (left) downward, (middle) neutral, or (right) upward next price movement prediction.

Table 4 shows the learning curves for each of the three labels corresponding to a

downward, neutral, or upward price movement. These learning curves, showing the F1 score on the training and test set against the size of the training set, are used to assess the bias-variance tradeoff of the feature set. Each training set, of size shown by the x-axis, is sampled from the full training set of balanced observations. The model is trained on this subset and the F1 score of each label is measured in-sample and out-of-sample. The sampling is repeated to infer a distribution for each of the in-sample and out-of-sample F1 scores. The mean and confidence band of the F1 scores, at one standard deviation, are shown in each plot.

Using the learning curve, the size of the training set is chosen so that the variance, that is the difference between the F1 score of the classifier on the training set and test set, is sufficiently low. The variance is observed to reduce with an increased training set size and suggests that the model is not-overfitting. The bias on the test set is also observed to reduce with increased training set size.



(a) DNN F1-score of $\hat{Y} = 1$ (b) DNN F1-score of $\hat{Y} = 0$ (c) DNN F1-score of $\hat{Y} = -1$.

Table 4: *The learning curves of the deep learner are used to assess the bias-variance tradeoff and are shown for (left) downward, (middle) neutral, or (right) upward price prediction. The variance is observed to reduce with an increased training set size and shows that the deep learning is not-overfitting. The bias on the test set is also observed to reduce with increased training set size.*

Figure 7 compares the observed ESU6 mid-price movements with the deep learner forecasted price movements over one 1 milli-second intervals between 12:22:20 and 12:24:20 CST. The bottom three panels show the corresponding probabilities of predicting each class. A probability threshold of 0.65 for the up-tick or down-tick classification is chosen here for illustrative purposes. Predicting the price movement protects high frequency market makers from adverse selection. False positives or negatives, when the observed mid-price is stationary, oftentimes result in unnecessary order cancellations and loss of queue position. The false prediction of a stationary mid-price, or a false positive (negative) when the observed mid-price is negative (positive) lead to adverse selection.

5 Discussion

Deep learning architectures stand out from other machine learning methods for their ability to handle complex interactions and nonlinearities. By viewing a spatio-temporal

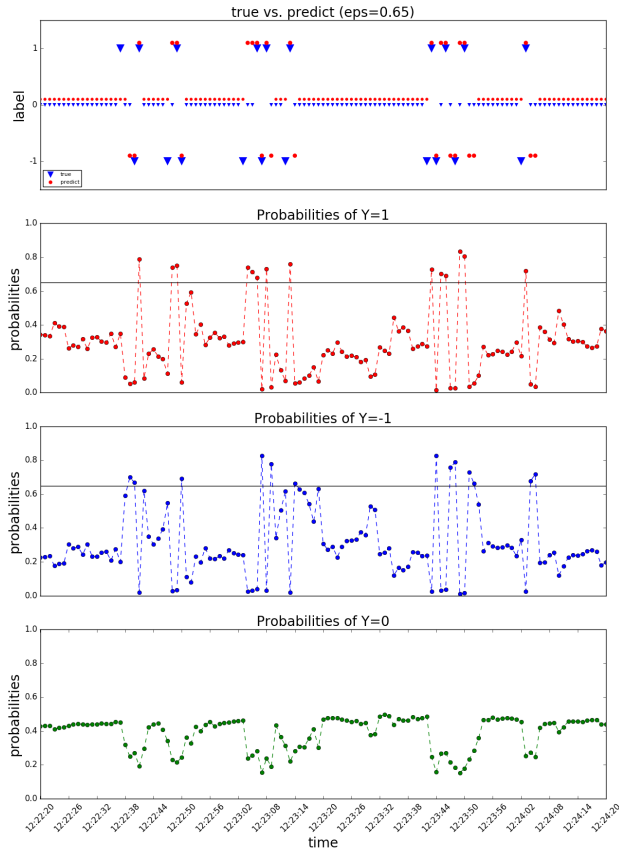


Figure 7: The (top) comparison of the observed ESU6 mid-price movements with the deep learner forecasted price movements over one milli-second intervals between 12:22:20 and 12:24:20 CST. The bottom three panels show the corresponding probabilities of predicting each class. A probability threshold of 0.65 for the up-tick or down-tick classification is chosen here for illustrative purposes.

dataset as 'image-like', we show the gains carry over to predicting sharp changes to spatial flow data in traffic and high frequency trading datasets.

There are many areas for future research. Given the temporal nature, studying more complex architectures than recurrent and feed-forward neural networks, and using neural Turing machines (NTMs) or long short-term memory (LSTMs) seems a very promising area for future statistical research. Finally, given the algorithmic nature of DL methods, understanding how they capture traditional physical models is also of interest. Much of the gains in other applied areas is the advantage of deep layers, see for example (Montúfar, Pascanu, Cho, & Bengio, 2014). Our work shows that this carries over to spatio-temporal modeling.

References

- Abadi, M., Barham, P., Chen, J., Chen, Z., Davis, A., Dean, J., et al. (2016). TensorFlow: A System for Large-scale Machine Learning. In *Proceedings of the 12th usenix conference on operating systems design and implementation* (pp. 265–283).
- Arnold, V. I. (1957). *On functions of three variables* (Vol. 114).
- Bastien, F., Lamblin, P., Pascanu, R., Bergstra, J., Goodfellow, I. J., Bergeron, A., ... Bengio, Y. (2012). *Theano: new features and speed improvements*. Deep Learning and Unsupervised Feature Learning NIPS 2012 Workshop.
- Bloomfield, R., O'Hara, M., & Saar, G. (2005). The "make or take" decision in an electronic market: Evidence on the evolution of liquidity. *Journal of Financial Economics*, 75(1), 165–199.
- Breiman, L. (2001). Statistical Modeling: The Two Cultures (with comments and a rejoinder by the author). *Statistical Science*, 16(3), 199–231.
- Cao, C., Hansch, O., & Wang, X. (2009). The information content of an open limit order book. *Journal of Futures Markets*, 29, 16–41.
- Cont, R., Kukanov, S., & Stoikov, S. (2014). The price impact of order book events. *Journal of Financial Econometrics*, 12, 47–88.
- Cressie, N., & Wikle, C. K. (2015). *Statistics for spatio-temporal data*. John Wiley & Sons.
- Dean, J., Corrado, G., Monga, R., Chen, K., Devin, M., Mao, M., ... others (2012). Large scale distributed deep networks. In *Advances in neural information processing systems* (pp. 1223–1231).
- Dixon, M., Klabjan, D., & Bang, J. H. (2016). Classification-based Financial Markets Prediction using Deep Neural Networks. *Algorithmic Finance*, to appear.
- Dobrislav, D., & Schaumburg, E. (2016). *High-frequency cross-market trading: Model free measurement and applications* (Tech. Rep.). Federal Reserve Bank of New York.
- Friedman, J., Hastie, T., & Tibshirani, R. (2010). Regularization paths for generalized linear models via coordinate descent. *Journal of Statistical Software*, 33(1), 1–22.
- Glorot, X., & Bengio, Y. (2010). Understanding the difficulty of training deep feedforward neural networks. In *In proceedings of the international conference on artificial intelligence and statistics (aistats'10)*. society for artificial intelligence and statistics.
- Gramacy, R. B., & Polson, N. G. (2011). Particle learning of gaussian process models for sequential design and optimization. *Journal of Computational and Graphical Statistics*, 20(1), 102–118.
- Heaton, J. B., Polson, N. G., & Witte, J. H. (2017). Deep learning for finance: deep portfolios. *Applied Stochastic Models in Business and Industry*, 33(1), 3–12.
- Higdon, D. (1998). A process-convolution approach to modelling temperatures in the north atlantic ocean. *Environmental and Ecological Statistics*, 5(2), 173–190.
- Horvitz, E. J., Apacible, J., Sarin, R., & Liao, L. (2012). Prediction, expectation, and surprise: Methods, designs, and study of a deployed traffic forecasting service. *arXiv:1207.1352*.
- Kolmogorov, A. N. (1957). On the representation of continuous functions of many variables by superposition of continuous functions of one variable and addition. *Dokl. Akad. Nauk SSSR*, 114, 953–956.

- Kozhan, R., & Salmon, M. (2012). The information content of a limit order book: the case of an FX market. *Journal of Financial Markets*, 15, 1–28.
- Montúfar, G., Pascanu, R., Cho, K., & Bengio, Y. (2014). On the Number of Linear Regions of Deep Neural Networks. In *Proceedings of the 27th international conference on neural information processing systems* (pp. 2924–2932). Cambridge, MA, USA: MIT Press.
- Nesterov, Y. (2013). *Introductory lectures on convex optimization: A basic course* (Vol. 87). Springer Science & Business Media.
- Nicholson, W. B., Matteson, D. S., & Bien, J. (2017). VARX-L: Structured regularization for large vector autoregressions with exogenous variables. *International Journal of Forecasting*, 33(3), 627–651. doi: <https://doi.org/10.1016/j.ijforecast.2017.01.003>
- Parlour, C. (1998). Price dynamics in limit order markets. *Review of Financial Studies*, 11, 789–816.
- Polson, N. G., & Sokolov, V. (2016). Deep learning predictors for traffic flows. *arXiv:1604.04527*.
- Polson, N. G., Willard, B. T., & Heidari, M. (2015). A statistical theory of deep learning via proximal splitting. *arXiv:1509.06061*.
- Richardson, R., Kottas, A., & Sansó, B. (2017). Flexible integro-difference equation modeling for spatio-temporal data. *Computational Statistics & Data Analysis*, 109, 182–198.
- Simon, N., Friedman, J., Hastie, T., & Tibshirani, R. (2011). Regularization Paths for Cox’s Proportional Hazards Model via Coordinate Descent. *Journal of Statistical Software*, 39(5), 1–13.
- Sirignano, J. (2016). Deep learning for limit order books. *arXiv:1601.01987*.
- Srivastava, N., Hinton, G. E., Krizhevsky, A., Sutskever, I., & Salakhutdinov, R. (2014). Dropout: a simple way to prevent neural networks from overfitting. *Journal of Machine Learning Research*, 15(1), 1929–1958.
- Stroud, J. R., Müller, P., & Sansó, B. (2001). Dynamic models for spatiotemporal data. *Journal of the Royal Statistical Society: Series B (Statistical Methodology)*, 63(4), 673–689. doi: 10.1111/1467-9868.00305
- Tran, D., Hoffman, D. M., Saurous, A. R., Brevdo, E., Murphy, K., & Blei, M. D. (2017). Deep probabilistic programming. *arXiv:1701.03757*.
- TransNet. (2016). *I-15 express lanes corridor*. ([online at <http://keepsandiegomoving.com/i-15-corridor/i-15-intro.aspx>; accessed 14-February-2016])
- Vlahogianni, E. I., Karlaftis, M. G., & Golias, J. C. (2005). Optimized and meta-optimized neural networks for short-term traffic flow prediction: a genetic approach. *Transportation Research Part C: Emerging Technologies*, 13(3), 211–234.
- Wikle, C. K., Milliff, R. F., Nychka, D., & Berliner, L. M. (2001). Spatiotemporal hierarchical bayesian modeling tropical ocean surface winds. *Journal of the American Statistical Association*, 96(454), 382–397.
- Zou, H., & Hastie, T. (2005). Regularization and variable selection via the elastic net. *Journal of the Royal Statistical Society Series B*, 67(2), 301–320.